Postprint of: Kaniewska K., Ponikiewski Ł., Szynkiewicz N., Cieślik B., Pikies J., Krzystek J., Dragulescu-Andrasi A., Stoian S., Grubba R.: Homoleptic mono-, di-, and tetra-iron complexes featuring phosphido ligands: a synthetic, structural, and spectroscopic study DALTON TRANSACTIONS Vol. 49, iss. 29 (2020), pp. 10091-10103
DOI: 10.1039/d0dt01503b

Homoleptic mono-, di-, and tetra-iron complexes featuring phosphido ligands: a synthetic, structural, and spectroscopic study.

Kinga Kaniewska[a], Łukasz Ponikiewski[a], Natalia Szynkiewicz[a], Bartłomiej Cieślik[b], Jerzy Pikies[a], J. Krzystek[c], Alina Dragulescu-Andrasi[d], Sebastian A. Stoian[e] and Rafał Grubba[a]*

We report the first series of homoleptic phosphido iron complexes synthesized by treating either the *β*-diketiminato complex [(Dippnacnac)$FeCl_2Li(dme)_2$] (Dippnacnac = HC[(CMe)N(C_6H_3-2,6-*i*Pr_2)]$_2$) or [$FeBr_2(thf)_2$] with an excess of phosphides R_2PLi (R = *t*Bu, *t*BuPh, Cy, *i*Pr). Reaction outcomes depend strongly on the bulkiness of the phosphido ligands. The use of *t*Bu_2PLi precursor led to an anionic diiron complex **1** encompassing a planar Fe_2P_2 core with two bridging and two terminal phosphido ligands. An analogous reaction employing less sterically demanding phosphides, *t*BuPhPLi and Cy_2PLi yielded diiron anionic complexes **2** and **3**, respectively, featuring a short Fe-Fe interaction supported by three bridging phosphido groups and one additional terminal R_2P^- ligand at each iron center. Further tuning of the P-substrates bulkiness gave a neutral phosphido complex **4** possessing a tetrahedral Fe_4 cluster core held together by six bridging *i*Pr_2P moieties. Moreover, we also describe the first homoleptic phosphanylphosphido iron complex **5**, which features an iron center with low coordination provided by three *t*Bu_2P-P$(SiMe_3)^-$ ligands. The structures of compounds **1**-**5** were determined by single-crystal X-ray diffraction and **1**-**3** by ^{1}H NMR spectroscopy. Moreover, the electronic structures of **1**-**3** were interrogated using zero-field Mössbauer spectroscopy and DFT methods.

Introduction

The development of ever faster, smaller, and smarter electronic devices requires advanced materials with pre-determined properties. This in turn causes a rapid growth in research of functional molecule-based materials. In this context, materials scientists are faced with a great demand to devise sustainable approaches to materials with targeted properties. Phosphorus-rich transition metal complexes are sought-after as potential platforms for many technologically relevant applications. Their synthesis, however, abiding the green chemistry principles for sustainability remains rather challenging. To this end, complexes of earth abundant, cheap and non-toxic transition metals in unique coordination environments have been pursued for their unique properties. Metal phosphides[1–7] represent one example of phosphorus-containing materials that show promise for many applications[2,7] including as electrochemical[8–12] and optoelectronic[13] devices. The majority of the recent reports have been concerned with phosphides' catalytic activity in promoting water-splitting reactions.[3,14–17] Phosphido ligands have a propensity to bridge two or more metal centers thereby forcing them in close proximity.[18] Because of this characteristic, phosphido ligands have attracted the interest of synthetic chemists for a long time and are among the best-known class of bridging ligands in coordination chemistry.[19–21] Despite of the high number of PR_2-containing compounds, there is only a limited number of examples of homoleptic phosphido complexes, and most contain main group metals[22] or lanthanides.[23,24] Up to now, the chemistry of homoleptic transition metal phosphido complexes has been explored by Hey-Hawkins and co-workers. They have successfully synthesized and structurally characterized several phosphorus rich compounds, starting from oligophosphanides[25–28], including iron.[29] They also reported the first homoleptic phosphido cobalt(III) complex [$K(thf)_4$][Co{1,2-(PtBu$_2$)$_2C_2B_{10}H_{12}$}$_2$][30] that can act as a precursor for metal phosphides. Furthermore, due to electrostatic differences between the PR_2 ligands and the ubiquitous amido groups, the phosphido complexes are attractive from both a synthetic and theoretical perspective as they could lead to products with novel chemical and magnetic properties. In this respect, particular attention has been paid to metal complexes with terminally coordinated phosphido moieties, especially for their involvement in hydrophosphination[31–43] and dehydrocoupling[32,44–46] reactions. Besides the use of noble and low-abundance metal compounds as intermediates in P-C and P-P bond formation processes[32,33,47–49], significant attention is

already being paid to iron complexes that could mediate such challenging transformations. Encouraged by results from Webster[50] and co-workers[51–57] we recently described the catalytic activity of terminal phosphido mono-iron complexes supported by β-diketiminato ligands in dehydrocoupling of secondary phosphines.[58] In addition to the catalytic potential shown by these mononuclear iron compounds, the chemistry of related phosphido diiron complexes offers key advantages related to the direct interaction between the two metal centers as well as the emulation of the active sites of [Fe-Fe] hydrogenases. Such diiron compounds are an interesting target to study not only for their unique structural motifs but also their reactivity[31,59,60], including the role as effective proton reduction electrocatalyst.[61–63] Thus, direct access to such compounds is very important.

In this paper we introduce a synthetic approach to unique iron homoleptic complexes featuring phosphido R_2P^- and phosphanylphosphido R_2P-(R')P^- ligands. In addition, we evaluate in detail the structural and spectroscopic characterization of a title compounds using X-ray diffraction and ^{1}H and Mössbauer spectroscopy.

Results and discussion

Syntheses

We have recently reported the synthesis of a novel family of terminal phosphido complexes of Fe(II) supported by a β-diketiminato ligand[58] by reacting [(Dippnacnac)$FeCl_2Li(dme)_2$][64] (Dippnacnac = HC[(CMe)N(C_6H_3-*2,6-i*Pr_2)]$_2$) with equimolar amounts of various phosphides R_2PLi. Motivated by our interest in iron complexes with phosphorus-rich coordination, we set out to prepare homoleptic iron complexes bearing R_2P^- ligands. To this end, we reacted the starting material, [(Dippnacnac)$FeCl_2Li(dme)_2$] or [$FeBr_2(thf)_2$] with an excess of R_2PLi (R_2P= *t*Bu_2P, *t*BuPhP, Ph_2P, Cy_2P, *i*Pr_2P). For these reactions, we selected phosphido ligands precursors with varied steric hindrance and electronic properties. Using this method we successfully synthesized a series of homoleptic complexes, which differ not only in the number and coordination mode of phosphido ligands but also in the number of iron centers which they enclose. Our studies revealed that the reaction outcome of lithium phosphides with starting Fe(II) complexes depends mainly on the electronic and steric properties of the phosphides. Reactions involving the most reducing *t*Bu_2PLi and *i*Pr_2PLi led to homoleptic metal clusters with a formal oxidation state for iron of +1.5, whereas reactions using less reducing *t*BuPhPLi or Cy_2PLi yielded homoleptic $Fe^{II}Fe^{II}$ diiron complexes. On the other hand, the reaction of metallic substrates with the most bulky *t*Bu_2PLi gave a homoleptic iron compound with four phosphido ligands, while reactions with less crowded phosphides such as *t*BuPhPLi, Cy_2PLi or *i*Pr_2PLi led to the formation of iron complexes bearing five or six phosphido ligands, respectively.

The reaction of [(Dippnacnac)$FeCl_2Li(dme)_2$] with three-fold molar excess of *t*Bu_2PLi in DME yielded an anionic diiron complex [Fe_2(*μ*-P*t*Bu_2)$_2$(P*t*Bu_2)$_2$][$Li(dme)_3$] (**1**) (Scheme 1).

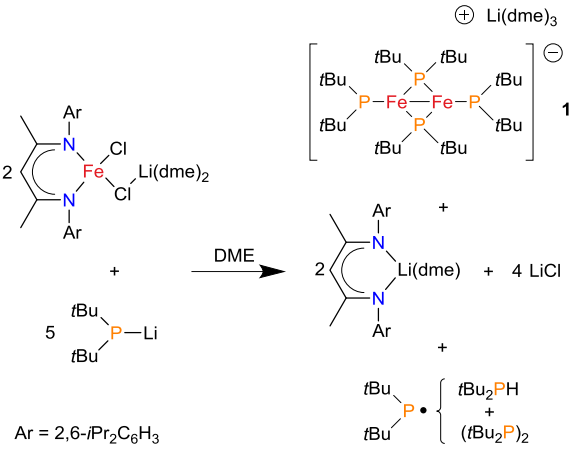

Scheme 1. Synthesis of the anionic phosphido complexes **1**.

The Dippnacnac ligand of the starting material was displaced from the iron coordination sphere and was isolated from the reaction mixture as [(Dippnacnac)Li(dme)], whose identity and structure was confirmed by ^{1}H NMR spectroscopy and X-ray crystallography. Complex **1** was isolated by fractional crystallization from concentrated DME solution at low temperature as X-ray quality dark-red crystals in 18% yield. The anionic character of **1** and the presence of two Fe centers and four *t*Bu_2P^- ligands indicate that the formal, average oxidation state of iron is +1.5. This suggests that a redox reaction occurs during synthesis such that one iron site is reduced and one phosphido group is oxidized to a phosphanyl radical. Indeed, the analysis of the reaction mixture $^{31}P\{^1H\}$ NMR spectra indicated the formation of significant amounts of *t*Bu_2PH as well as trace amounts of (*t*$Bu_2P)_2$, which could be ascribed as products of reactions of the *t*Bu_2P· radical with either the solvent or themselves (dimerization), respectively (Figure S4).

Reactions of [(Dippnacnac)$FeCl_2Li(dme)_2$] with less crowded phosphides, such as *t*BuPhPLi or Cy_2PLi, led to the formation of diiron anionic complexes [Fe_2(*μ*-PR_2)$_3$(PR_2)$_2$][$Li(dme)_3$] (R_2P= *t*BuPhP (**2**), Cy_2P (**3**)) with five phosphido ligands coordinated to a Fe-Fe core (Scheme 2).

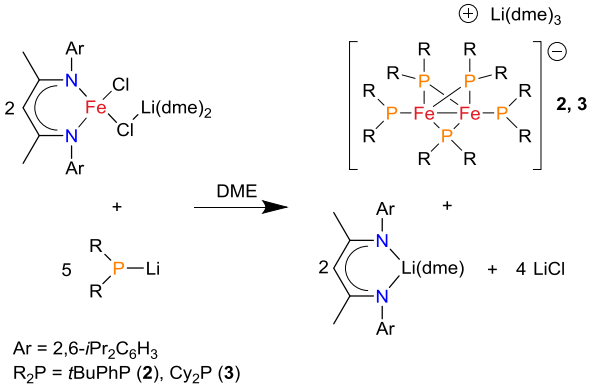

Scheme 2. Syntheses of complexes **2** and **3**.

As in the case of complex **1**, the synthesis of **2** and **3** is accompanied by the formation of [(Dippnacnac)Li(dme)] and LiCl, which could be removed from the reaction mixture by

fractional crystallization. Whereas **2** was isolated as black crystals (yield 39%) from concentrated DME solution layered with pentane at room temperature, **3** was obtained as dark violet crystals in high yield (86%) from concentrated DME solution at low temperature. However, in contrast to **1**, the formal oxidation state of iron sites of **2** and **3** is +2, thus maintaining the same oxidation state as in the Fe(II) starting material. Despite this fact, signals attributed to R_2PH and $(R_2P)_2$ were visible in the $^{31}P\{^1H\}$ NMR spectra of reaction mixtures (Figures S6 and S8). This observation suggests that other redox side-reactions accompany the main process taking place in the solution.

Interestingly, reacting the *i*Pr_2PLi phosphide, which has less sterically demanding substituents in comparison to other ligand precursors, with [(Dippnacnac)$FeCl_2Li(dme)_2$] in a molar ratio 3:1 yielded a tetrairon neutral phosphido complex [$Fe_4(\mu$-P*i*$Pr_2)_6$] (**4**) (Scheme 3).

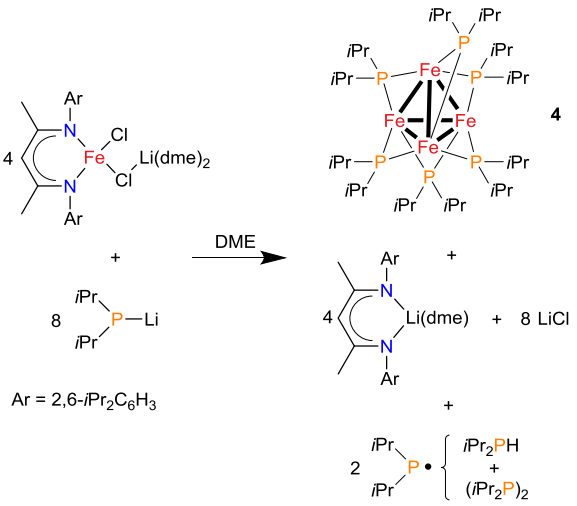

Scheme 3. Synthesis of complex **4**.

Complex **4** features a tetrahedral Fe_4 core held together by six *i*Pr_2P^- bridging ligands. These structural features indicate that each iron center has a formal, average oxidation state of +1.5. Similar to **1**, the phosphido group is possibly acting as a reducing agent being oxidized to the corresponding phosphanyl radical. This is supported by the $^{31}P\{^1H\}$ NMR spectra of the reaction mixture, where a strong signal assigned to *i*Pr_2PH and signal from $(iPr_2P)_2$ were observed (Figure S10). X-ray quality black crystals of **4** were obtained in moderate yield (58 %) from concentrated pentane solutions at -70°C.

Reactions of [(Dippnacnac)$FeCl_2Li(dme)_2$] with an excess of Ph_2PLi did not yield homoleptic phosphido complexes. In contrast to the reactions described above, the (Dippnacnac) ligand was not replaced in the coordination sphere of iron and thus the main product was the heteroleptic diphosphido complex [(Dippnacnac)$Fe(PPh_2)_2$][$Li(dme)_3$].[58]

The successful isolation of the series of homoleptic iron complexes with phosphide ligands prompted us to investigate the use of phosphanylphosphido R_2P-(R')P^- ligands with the goal of obtaining homoleptic complexes. In comparison to classical phosphido ligands, phosphanylphosphido ligands have one of R substituents replaced by a phosphanyl group. The presence of an additional P-donor atom may result in the side-on coordination of the phosphanylphosphido ligand to the metal center. We have previously reported several heteroleptic transition metal complexes with such ligands[65–72] including terminal and side-on complexes of Fe(II).[73] However, to the best of our knowledge, homoleptic complexes of transition metals bearing R_2P-PR' moiety have not yet been described in the literature. We were content to obtain the homoleptic complex [$Fe(\eta^1$-Me_3SiPP-*t*$Bu_2)_3$][$Li(dme)_3$] (**5**) from [(Dippnacnac)$FeCl_2Li(dme)_2$] and an excess of *t*Bu_2P-P($SiMe_3$)Li (Scheme 4). As observed in the syntheses of homoleptic phosphido complexes, [(Dippnacnac)Li(dme)] and LiCl are side products of this reaction. Formally, the iron site of **5** has the same oxidation state as that of the Fe(II) starting material. Dark brown crystals of **5** were obtained in 32% yield by slow diffusion of pentane into concentrated DME solution at room temperature.

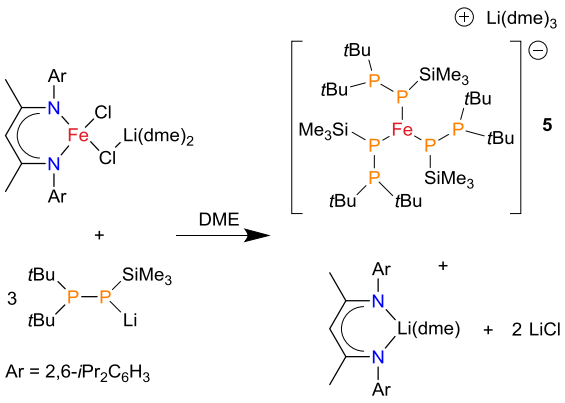

Scheme 4. Synthesis of phosphanylphosphido complex **5**.

In the next step, in order to streamline our synthetic approach, we turned our attention to the use of [$FeBr_2(thf)_2$] as a starting material for the synthesis of homoleptic iron complexes. As shown in Scheme 5, homoleptic phosphido complexes **1-4** were obtained using a simple, straightforward method by reacting [$FeBr_2(thf)_2$] with an excess of phosphides R_2PLi (R = *t*Bu, *t*BuPh, Cy, *i*Pr) in DME. In this case, we have tested different molar ratio of reagents (1:3, 1:4, and 1:6) (see Table S3 for details). The yields of **1** and **2** were even higher than those obtained for the reactions with [(Dippnacnac)$FeCl_2Li(dme)_2$] (65% *vs* 18% for **1**; and 64% vs 39%, for **2**). However, the syntheses of **3** and **4** using [$FeBr_2(thf)_2$] were less effective with yields significantly lower than those obtained when [(Dippnacnac)$FeCl_2Li(dme)_2$] was used as a starting material (8% vs 86% for **3**; 3% vs 58% for **4**). These experiments indicate that these two synthetic methods to yield homoleptic phosphido iron complexes are complementary. Unfortunately, reactions of [$FeBr_2(thf)_2$] with an excess of Ph_2PLi or *t*Bu_2P-P($SiMe_3$)Li did not produce isolable products.

Complexes **1**-**5** are air-sensitive and should be handled under an Ar atmosphere. The most prone to oxidation and hydrolysis are complexes **4** and **5**; the former has the least bulky

phosphido groups (*i*Pr_2P), whereas the latter possesses very reactive phosphanylphosphido moieties.

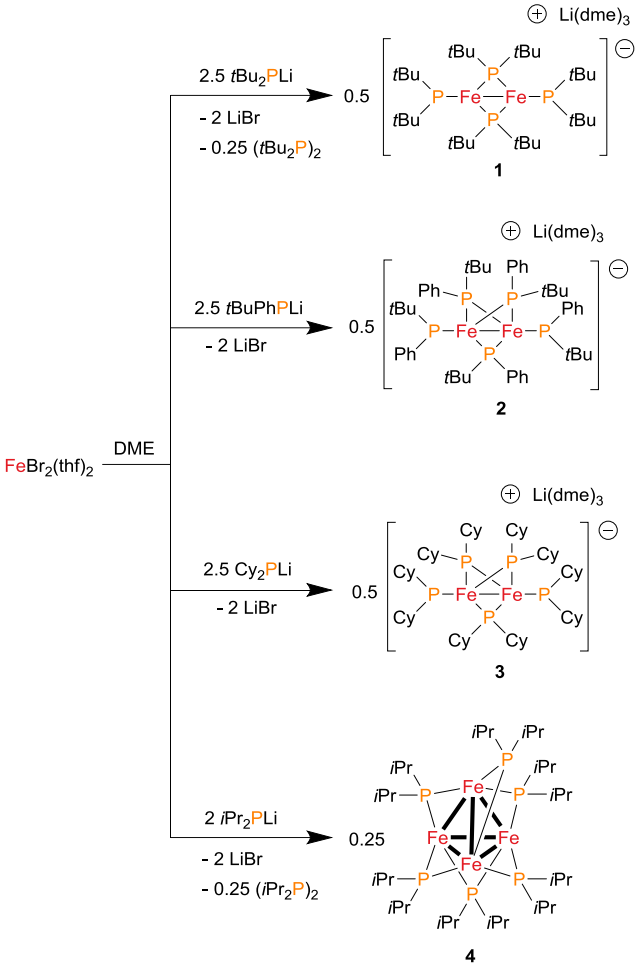

Scheme 5. Syntheses of homoleptic phosphido complexes **1-4** from $[FeBr_2(thf)_2]$.

Crystal structures

Single-crystal X-ray analysis confirmed that **1**-**5** are the first examples of homoleptic iron complexes with PR_2^- phosphido ligands. The molecular structure of a complex anion **1** and its important metric parameters are shown in Figure 1 and Table 1, respectively.

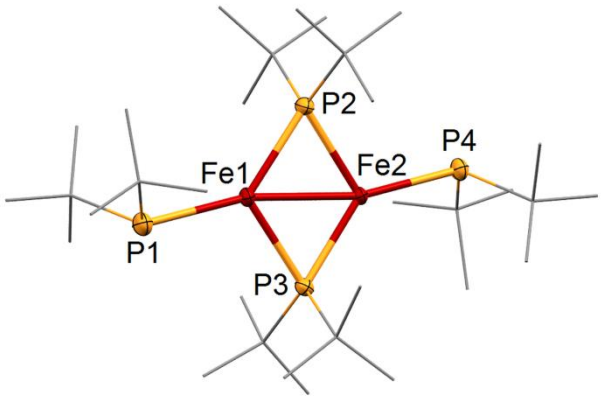

Figure 1. The X-ray structure of complex anion **1** showing the atom-numbering scheme. Ellipsoids are shown at 50% probability. H atoms, and $[Li(dme)_3]^+$ counterion are omitted for clarity.

Table 1. Selected bond lengths and geometries around iron and phosphorus atoms for complex **1**.

No.	Fe1-Fe2 (Å)	Fe1-P1[a] Fe2-P4[a] (Å)	Fe1-P2[b] Fe2-P2[b] Fe1-P3[b] Fe2-P3[b] (Å)	ΣP1[a] ΣP2[b] ΣP3[b] ΣP4[a] (°)	ΣFe1[c] ΣFe2[c] (°)
1	2.6034(5)	2.4176(7) 2.4196(7)	2.2654(7) 2.2737(7) 2.2792(7) 2.2670(7)	328.09 417.44 417.69 327.99	360.00 359.99

[a] terminal P-atoms; [b] bridging P-atoms; [c] neglecting Fe-Fe bonding

Compound **1** crystalizes as a complex anion with a lithium cation solvated by three DME molecules. The complex anion **1** contains a mixed-valent $[Fe_2]^{3+}$ core to which four tBu_2P groups are coordinated. Two ligands are bridging the two metal centers whereas the remaining ones act as terminal ligands. The Fe1-Fe2 distance of 2.6034(5) Å is typical for Fe-Fe single bonds supported by phosphido ligands.[31,74–81] The Fe-P bonds of the terminal ligands are about 0.15 Å longer than the corresponding distances observed for the bridging phosphido groups (Table 1). In contrast to the heteroleptic complex with π-acidic CO auxiliary ligands $[Fe_2(CO)_5(\mu\text{-}tBu_2P)_2]$[82], Fe-P distances of the bridging phosphido groups are almost equal (~2.27 Å); these bonds are of intermediate length in comparison to those observed for $[Fe_2(CO)_5(\mu\text{-}tBu_2P)_2]$[82] (Fe1-P: 2.3687(8) Å; Fe2-P: 2.1368(8) Å). Most of the known iron complexes with the Fe-Fe bond supported by two phosphido ligand exhibit a butterfly Fe_2P_2 core structure where the core is folded about the Fe-Fe bond or about the P···P vector.[79–81,83,84] Fewer examples of heteroleptic complexes contain a planar Fe_2P_2 core.[75,77,79,83,85,86] Complex **1** features a similar core with Fe1, Fe2, P2, and P3 atoms forming a planar ring. Moreover, two P-atoms of the terminal ligands are coplanar with this ring. The bond vectors Fe1-P1, Fe2-P2 and Fe1-Fe2 are not collinear and P1-Fe1-Fe2 and Fe1-Fe2-P4 bond angles are ~167°. The geometries at Fe1 and Fe2 are trigonal planar, not considering the Fe1-Fe2 bond (Table 1). The geometries of bridging P-ligands are tetrahedral, whereas the terminal ones are pyramidal, as expected. The long Fe-P distances of the terminal ligands together with their pyramidal geometry indicate that there is no interaction between the lone pairs at P atoms and the Fe centers.

Complexes **2** and **3** are structurally similar and will be discussed together. The molecular structure of complex anions **2** and **3** are depicted in Figures 2 and 3, respectively. The most important metric parameters of **2** and **3** are included in Table 2. In the case of **2** and **3**, the influence of the steric effect of phosphido ligands on the structure is clearly visible. In contrast to **1**, which bears more bulky tBu_2P groups, compounds **2** and **3** contain five R_2P moieties coordinated to the $[Fe_2]^{4+}$ core. Two of the phosphido groups display terminal coordination whereas the other three act as bridging ligands. To the best of our knowledge, **2** and **3** are the first examples of complexes with a

Fe-Fe bond supported by three R_2P groups. The most striking structural feature of both **2** and **3** is their short Fe1-Fe2 distance of 2.3682(7) Å and 2.3743(8) Å, respectively. According to the Cambridge Structural Database (CSD), these Fe-Fe bonds are the shortest ones supported by phosphido ligands.[87] Unlike **1**, complexes **2** and **3** have comparable Fe-P(terminal) and Fe-P(bridging) distances (Table 2). The geometry at each Fe center is distorted tetrahedral (not considering the Fe-Fe bond). As observed for **1**, the terminal phosphido ligands are pyramidal whereas the bridging R_2P groups possess tetrahedral geometry. The flap angles between the Fe_2P(bridging) planes are nearly identical in **2** (119.38°, 119.92°, 120.70°) but less similar in **3** (125.45°, 118.21°, 116.34°). Similarly to **1**, the Fe-P(terminal) and Fe-Fe bond vectors are not collinear in case of **2**-**3**, where the Fe-Fe-P(terminal) angle falls in the 158.49-162.96° range.

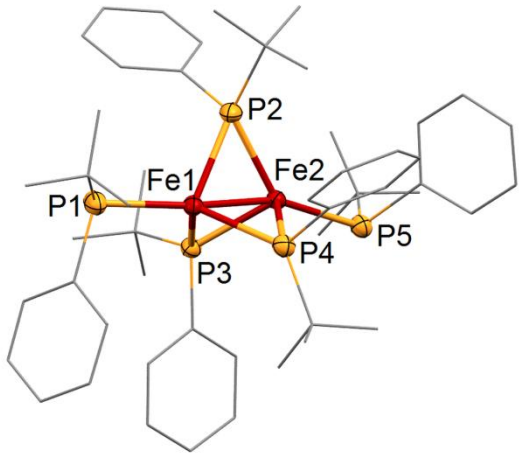

Figure 2. The X-ray structure of the complex anion **2** showing the atom-numbering scheme. Ellipsoids are shown at 50% probability. H atoms, $[Li(dme)_3]^+$ counterion, and DME molecule are omitted for clarity.

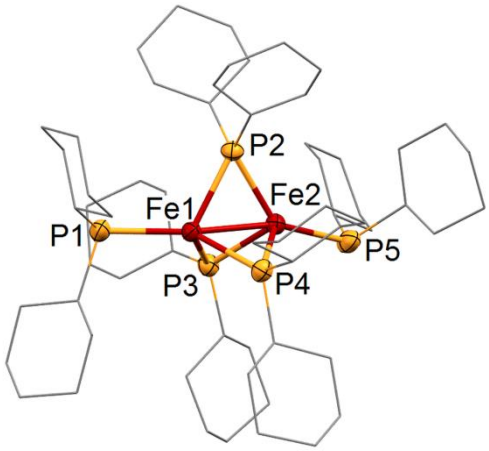

Figure 3. The X-ray structure of the complex anion **3** showing the atom-numbering scheme. Ellipsoids are shown at 50% probability. H atoms, $[Li(dme)_3]^+$ counterion, and DME molecule are omitted for clarity.

Table 2. Selected bond lengths and P-atom geometries in complexes **2** and **3**.

No.	Fe1-Fe2 (Å)	Fe1-P1[a] Fe2-P5[a] (Å)	Fe1-P2[b] Fe2-P2[b] Fe1-P3[b] Fe2-P3[b] Fe1-P4[b] Fe2-P4[b] (Å)	ΣP1[a] ΣP5[a] (°)	ΣP2[b] ΣP3[b] ΣP4[b] (°)
2	2.3682(7)	2.368(1) 2.377(1)	2.378(1) 2.338(1) 2.355(1) 2.3230(9) 2.345(1) 2.3559(9)	321.79 316.59	400.48 404.01 403.87
3	2.3743(8)	2.351(1) 2.353(2)	2.338(1) 2.304(1) 2.305(2) 2.325(2) 2.323(1) 2.359(2)	323.89 323.15	413.56 417.55 405.14

[a] terminal P-atoms; [b] bridging P-atoms

The Fe-Fe distances in **1**, **2** and **3**, with values of 2.6034(5) Å, 2.3682(7) Å and 2.3743(8) Å which are within 2.20-2.69 Å range reported for diiron complexes with significant metal-metal interactions, resulting in a Fe-Fe single bonding.[88,89,90,91,92,93,94,95] Moreover, the metal-metal distances observed for **2** and **3** are very close to the sum of two single covalent bond radii for Fe atom (2.32 Å).[96] Although the short Fe-Fe distances of **1**-**3** suggest the presence of metal-metal bonding in these complexes, on its own this feature is not sufficient proof of an intermetallic bond formation. Our calculations indicate significant metal-metal interaction in **1**-**3** (see section *DFT calculations* for details).

The neutral complex **4** crystallizes in the space group $R\bar{3}$ (point group S_6) indicating a high molecular symmetry for this compound. The molecular structure of **4** is shown in Figure 4 and selected geometric parameters of **4** are given in Table 3.

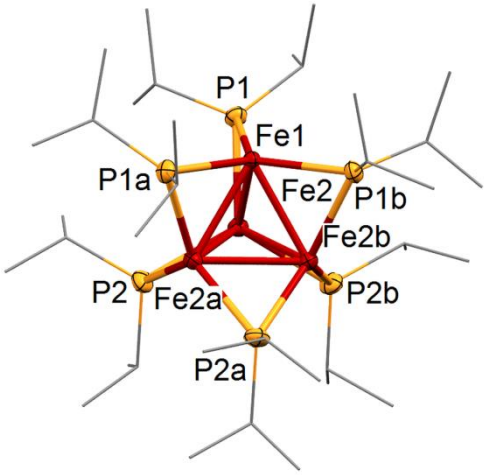

Figure 4. The X-ray structure of the complex **4** showing the atom-numbering scheme. Ellipsoids are shown at 50% probability. H atoms, and pentane molecule are omitted for clarity.

Table 3. Selected bond lengths and geometries at iron and phosphorus atoms for complex **4**.

No.	Fe1-Fe2 Fe2-Fe2a (Å)	Fe1-P1 Fe2-P1 Fe2-P2 (Å)	ΣP1 ΣP2	ΣFe1[a] ΣFe2[b] (°)
4	2.4058(5) 2.4007(6)	2.2724(6) 2.2845(7) 2.2856(7)	407.45 415.47	358.86 358.94

[a] Sum of angles: P1-Fe1-P1a, P1a-Fe1-P1b, P1b-Fe1-P1; [b] Sum of angles: P1-Fe2-P2, P2-Fe2-P2b, P2b-Fe2-P1

The mixed-valent $[Fe_4]^{6+}$ tetrahedron constitutes the core of the complex. In contrast to the other homoleptic phosphido complexes discussed above, in **4** all *i*Pr_2P groups act as bridging ligands. Each of the *i*Pr_2P groups bridges two Fe atoms and the complex has a symmetrical arrangement of the phosphido bridges. Each Fe atom and three P-atoms from the coordinated ligands are almost coplanar (Table 3), thus the geometry of Fe atoms in **4** can be described as planar trigonal (neglecting the Fe-Fe bonds). As expected, the geometry of the bridging P-atoms is tetrahedral. The average Fe-Fe bond length of 2.4033 Å is significantly shorter than corresponding distances in the diiron complex **1** (2.6034(5) Å), but only slightly longer than the Fe-Fe bond distance in **2** and **3** (2.3682(7) Å and 2.3743(8) Å, respectively). According to CSD, the Fe-Fe bond lengths in **4** are shorter than any reported for complexes with a tetrahedral Fe_4 core.[87] The Fe-P distances (av. 2.281 Å) are similar to the corresponding distances involving the bridging ligands of **1** (av. 2.271 Å) but considerably shorter than Fe-P(bridging) distances in **2** and **3** (av. 2.337 Å).

The structure of anionic complex **5** is presented in Figure 5 and its important geometric parameters are collected in Table 4.

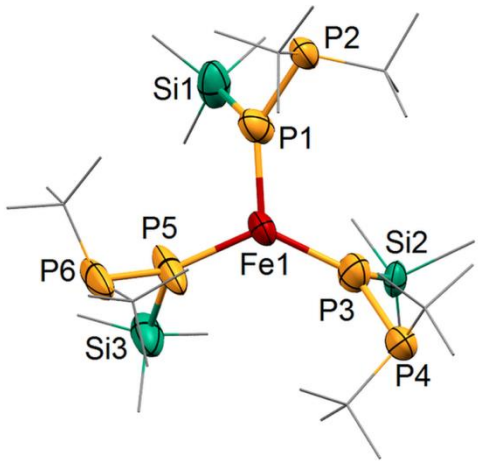

Figure 5. The X-ray structure of the complex anion **5** showing the atom-numbering scheme. Ellipsoids are shown at 50% probability. H atoms, and $[Li(dme)_3]^+$ counterion are omitted for clarity.

Table 4. Selected bond lengths and geometries of iron and phosphorus atoms in complex **5**.

No.	Fe1-P1 Fe1-P3 Fe1-P5 (Å)	P1-P2 P3-P4 P5-P6 (Å)	P1-Si1 P3-Si2 P5-Si3 (Å)	ΣFe1 ΣP1 ΣP3 ΣP5 (°)	ΣP2 ΣP4 ΣP6 (°)
5	2.346(1) 2.345(1) 2.334(2)	2.167(2) 2.167(2) 2.167(2)	2.199(2) 2.19(2) 2.182(2)	358.87 356.59 354.13 357.78	319.83 319.31 320.09

The geometry of the Fe center can be described as trigonal planar, with three terminal phosphido P-atoms of *t*Bu_2P-$PSiMe_3^-$ ligands coordinated to Fe. Interestingly, the geometries of the terminal P-atoms P1, P2 and P3 are nearly planar, whereas geometries around phosphanyl P-atoms are pyramidal. The bond distances Fe-P and P-P distances (av. 2.342 Å and 2.166 Å, respectively) are very similar to the corresponding distances reported by us for the heteroleptic complex [(Dippnacnac)Fe(η^1-Me_3SiPP-*t*Bu_2)] (2.3144(17) Å and 2.168(2) Å, respectively).[73] These long Fe-P distances have essentially single bond character.[97] Otherwise, the P-P distances are shorter than the typical single P-P bond (the sum of single bond covalent radii for two P is 2.22 Å).[96] Together with the planar geometry of P-phosphido atoms, this observation suggests that the lone pairs located on these atoms are involved in interactions with the phosphanyl P-atoms increasing the π-character of the P-P bonds within phosphanylphosphido ligands. The diphosphorus ligands exhibit an anticlinal conformation with absolute values of the torsion angles C-P-P-Si in the 112.6°-131.84° range. The phosphanyl and trimethylsilyl groups are located on opposite sides of the molecule with respect to the P1P3P5 plane.

^{1}H NMR spectroscopy

Despite of the paramagnetic character of **1**-**3**, the structures of these complexes in solution were investigated by NMR spectroscopy. It was previously reported, that in case of ^{1}H NMR spectra of paramagnetic Fe(II) complexes the integration can be very useful in the signal assignment.[98] ^{1}H NMR spectra of concentrated THF-d_8 solutions of **1**-**3** are very simple and contain only broad signals which correspond to phosphido ligands, signals of DME, residual signals of THF-d_8 and a very weak signal of hydrolysis product of R_2PH. The ^{1}H NMR spectrum of **1** displays two broad resonances at 23.76 ppm and at -22.48 ppm with integral numbers 1/1 (Figure S1). This is consistent with the presence of an equal number of the bridging and terminal phosphido ligands in **1**. In contrast to the ^{1}H NMR spectrum recorded for **1**, complex **3** shows four broad resonances at 22.67 ppm, 11.63 ppm, 0.43 ppm, and -0.66 ppm (Figure S3). The first two mentioned signals with integral numbers 36/24 can be attributed to CH_2 groups of bridging Cy_2P^- ligands, whereas the last two resonances with integral numbers 24/16 can be ascribed to CH_2 groups of terminal Cy_2P^- ligands. The signals of CH groups of cyclohexyl rings are not visible because of the presence of paramagnetic Fe centers in

the close vicinity. The ^{1}H NMR spectrum recorded for **2** exhibits six broad signals (Figure S2). The greater number of signals observed in ^{1}H NMR spectra of **2** can be explained by the structural feature of this complex, where two different substituents (*t*Bu and Ph) are bound to P atoms. Three signals at 39.79 ppm, 23.70 ppm, 20.23 ppm can be assigned to the *t*Bu groups and aromatic protons of bridging phosphido ligands with their integral numbers equal to 27/9/6. Moreover, three other resonances at 6.83 ppm, 1.32 ppm, and -9.80 ppm of terminal phosphido groups are also visible. Based on their integral numbers with values of 4/18/6, the signals at 6.83 ppm and -9.80 ppm can be ascribed to CH protons of phenyl rings, whereas the integration of signal at 1.32 ppm is in a line with the number of *t*Bu group protons of terminal phosphido ligands. It is worth to mention that **1**-**3** could not be studied by ^{31}P NMR spectroscopy due close proximity of the P atoms to paramagnetic Fe centers. The ^{1}H NMR results are in accordance with X-ray data for complexes **1**-**3** and confirm that these complexes exhibit similar structures both in solid state and in solution.

Magnetic susceptibility measurements

The magnetic moments of **1**-**3** in solution were determined using the Evans method.[99,100] The obtained values of magnetic moments μ_{eff} are 5.66 μ_B, 6.96 μ_B, and 6.89 μ_B for **1**, **2** and **3**, respectively. The measured magnetic moment of **1** is in fairly good agreement with the predicted magnetic moment that equals 5.92 μ_B for an interacting diiron center with S = 5/2. On the other hand, the obtained values of magnetic moments for **2** and **3** are in very good accordance with calculated value of 6.93 μ_B for a diiron system with S = 3. The postulated spin states for complexes **1** and **2**, **3** are significantly reduced in comparison to expected values for a high-spin $Fe^{I}Fe^{II}$ system (S = 7/2) and a high-spin $Fe^{II}Fe^{II}$ system (S = 4). The reduction of magnetic moments and spin states in case of **1**-**3** can be explained by a strong antiferromagnetic coupling of the two iron centers or by a presence of a Fe-Fe bond. Floriani and co-workers reported several diiron complexes where a reduction of spin states and magnetic moments was observed.[89] They obtained a $Fe^{II}Fe^{II}$ dimeric homoleptic iminoacyl complex, [{η^2-C(Mes)=NBut}$_2$Fe$_2${η^2-C(Mes)=NBut}$_2$], which exhibits a S = 3 spin state and possesses a single Fe-Fe bond. Interestingly, the Fe-Fe bond distance in aforementioned complex is very short (2.371(4) Å) with almost the same value as corresponding distances in **2** and **3** (Table 2). Lu and co-workers reported the synthesis of [Fe$_2$Cl(py$_3$tren)] (py$_3$tren = N,N,N-tris(2-(2-pyridylamino)ethyl)amine), which exhibits the same $Fe^{II}Fe^{II}$ core and spin state as **2** and **3**; however, it has a slightly shorter Fe-Fe distance with value of 2.2867(5) Å.[95]

DFT calculations

Further insight into the structural features and metal-metal interactions in **1**-**3** was provided by density functional theory (DFT) and natural bond orbital (NBO) calculations. These results indicate that a sextet and septet ground state is favored for **1** and **2**-**3**, respectively (Table S5), which is compatible with the experimental values of magnetic moments recorded for the aforementioned complexes. DFT calculations show that the positions of highest spin density are located at iron atoms with almost equal spin distribution between both iron centers (Table 5, Figures S14, S16 and S18). Moreover, significantly smaller contribution of a spin density was found at P-atoms of phosphido ligands. NBO analysis confirms a presence of a σ-single metal-metal bond in **1**-**3** resulting from overlapping two d_{z^2} orbitals of Fe atoms. The NBO orbitals attributed to the Fe-Fe bond in **1**-**3** are depicted in Figure 6. The Mayer bond orders (MBO) calculated for the Fe-Fe bonds in **1**, **2** and **3** are 0.377, 0.482 and 0.494, respectively, and suggest bond order significantly lower than 1. Complex **1** displays the lowest value of MBO for the Fe-Fe bond which is in accord with longer metal-metal distance in comparison to corresponding distances observed in **2** and **3** (Table 2).

Table 5. Calculated Mayer bond orders (MBO) for Fe-Fe bonds and spin densities on two Fe centers in complexes **1**-**3**.

No.	MBO Fe1-Fe2	NBO spin density		
		Fe1	Fe2	P1 P2 P3 P4 P5
1	0.377	2.785	2.833	-0.124 -0.201 -0.202 -0.140
2	0.482	2.857	3.074	-0.150 0.014 0.003 0.098 0.000
3	0.494	2.979	2.940	-0.056 0.051 -0.019 0.112 -0.101

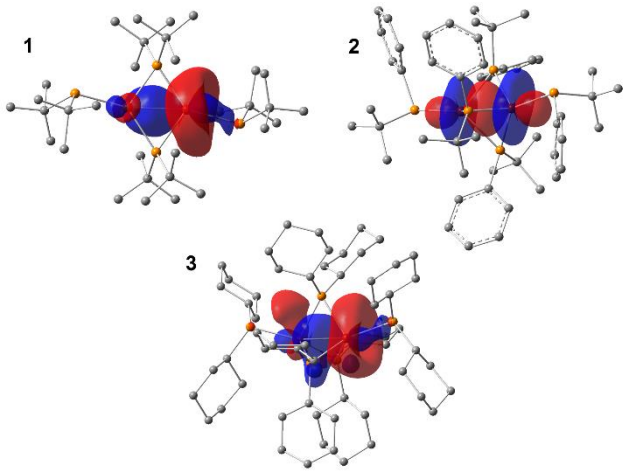

Figure 6. Calculated Fe-Fe natural bond orbitals (NBO) of **1**-**3**.

^{57}Fe Mössbauer spectroscopy

The electronic structures of **1**-**3** were investigated by recording of a series of zero-field Mössbauer spectra at 80 K. The spectrum recorded for **1** exhibits a symmetric, well-defined quadrupole doublet that accounts for more than 95% of the iron present in the sample, see Figure 7. The observation of a single doublet suggests that the two iron sites have identical electronic environments and that **1** is a fully delocalized, mixed-valent species. This behaviour is similar to that observed for the analogous mixed-valent complex $Fe_2(DPhF)_3$ reported by Lu and co-workers (DPhF = diphenylforamidinate).[101] While the isomer shift values of **1** and $Fe_2(DPhF)_3$ are rather similar, the quadrupole splitting of **1** is considerably larger (Table 6). Most likely, the latter difference originates with the lower symmetry of iron sites of **1** which, possibly, induces a misalignment of the ligand and valence contributions of the electric field gradient tensors.[102] Interestingly, advanced quantum mechanical calculations performed for $Fe_2(DPhF)_3$ showed that the $[Fe_2]^{3+}$ core is best described considering a coherent superposition of Fe(II) and Fe(I) wavefunctions.

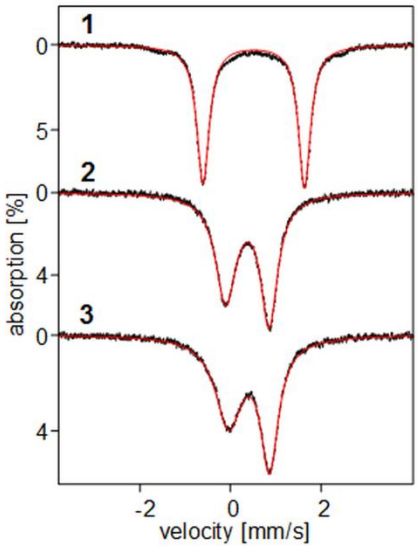

Figure 7. Zero-field Mössbauer spectra recorded at 80 K for complex **1**, **2**, and **3**. The solid red lines are simulations obtained using the parameters listed in Table 5.

Compared to **1** the increase in the charge of the $[Fe_2]$ moiety of **2** and **3** leads to lower isomer shift and quadrupole splitting values. Although this behaviour is consistent with an increase in the oxidation state of the iron cluster, these values are lower than those of typical high-spin ferrous complexes. In particular, the isomer shift is considerably lower than anticipated. This observation suggests that the iron-iron bonding interaction leads to a significant mixing of the $3d_{z^2}/4s$ orbitals and, in turn, to a boost in the population of the excited 4*s* atomic orbitals of the iron ions. Additionally, the resonances for these spectra are unusually broad, with a linewidth Γ = 0.5-0.7 mm/s vs a typical value of 0.30 mm/s. The asymmetry and the broadness of these quadrupole doublets is probably a diagnostic for the presence of an unresolved magnetic hyperfine splitting. For integer spin systems such as **2**-**3**, particularly for large S values, this behaviour is typically associated with the presence of a vanishing zero-field splitting of a $|S, M_S\rangle \approx |S, \pm S\rangle$ ground quasi-doublet.[103] While for half-integer spin systems the Kramers theorem specifies that spin sublevels must be doubly-degenerate in zero-field, for integer spin systems the same theorem indicates that spin sublevels should be energetically separated from one another. However, two lowest spin sublevels $|S, M_S\rangle \approx |S, \pm S\rangle$ for **2**-**3** are, most likely, nearly degenerate which, in turn, leads to a quasi-doublet ground state.

Table 6. Mössbauer parameters used to simulate the spectra of Figure 6.

Complex	δ [mm/s]	ΔE_Q [mm/s]	Γ (L/R) [mm/s]	Area [%]	Ref.
1	0.515(3)	2.224(2)	0.33/0.32	96(2)	this work
$Fe_2(DPhF)_3$	0.65	0.32	n.a.		91
2	0.37(2)	0.96(2)	0.55/0.46	100(3)	this work
3	0.41(1)	0.90(1)	0.71/0.46	100(3)	

Conclusions

Reactions of lithium phosphides R_2PLi with $[(Dippnacnac)FeCl_2Li(dme)_2]$ or $[FeBr_2(thf)_2]$ constitute successful and complementary methods for obtaining homoleptic phosphido complexes of iron. The structures of resulting compounds can be easily tuned by selecting phosphido ligands differing in the bulkiness of the R_2P moiety, which leads to Fe-, Fe_2- and Fe_4-core complexes. A ^{57}Fe Mössbauer spectroscopy analysis of diiron compound **1** confirms low oxidation state of Fe and indicates that this complex is a fully delocalized, mixed-valent Fe^{I}/Fe^{II} species. Unprecedented structural features of **2** and **3**, where Fe-Fe bond is supported by three R_2P groups result in very short Fe-Fe bond distances and according to ^{57}Fe Mössbauer spectroscopy in strong $3d_{z^2}/4s$ orbital interactions. DFT calculations performed for **1**-**3** confirm the presence of Fe-Fe σ-bonds in these complexes, which result from overlapping $3d_{z^2}$ orbitals of both metallic centers.

Experimental part

Materials and methods

All manipulations were performed under an Ar atmosphere in flame-dried Schlenk-type glassware on a vacuum line or in a dry box. Solvents were dried by standard methods (1,2-dimethoxyethane (DME) was dried with K/benzophenone; pentane was dried with Na/benzophenone/dyglime) and distilled under argon. $FeBr_2$ was purchased from Aldrich. Literature methods were used to prepare phosphides R_2PLi (R = *i*Pr, *t*Bu, Cy, *t*BuPh)[58] and $[(Dippnacnac)FeCl_2Li(dme)_2]$[64]. The synthesized compounds are very moisture- and air-sensitive.

$^{31}P\{^1H\}$ NMR (external standard 85% H_3PO_4), ^1H (internal standard Me_4Si) spectra were recorded on a Bruker AV400 MHz spectrometer at room temperature. Data were processed using

Bruker's Topspin 3.5 software. ^{1}H NMR spectroscopic measurements of magnetic susceptibility used the Evans method[99] and were corrected for diamagnetism[100].

Diffraction data of complexes **2**-**4** were collected on a diffractometer equipped with a STOE image plate detector using Mo$K\alpha$ radiation with graphite monochromatization (λ = 0.71073 Å). Good quality single-crystal specimens were selected for the X-ray diffraction experiments at 120 K for complexes **2-4**. The experimental diffraction data of **1** was collected on a Gemini S-Ultra single crystal CCD diffractometer from Oxford Diffraction equipped with a CryojetHT-temperature system using Cu$K\alpha$ (λ = 1.54184 Å) radiation with mirror monochromatization. The X-ray crystallographic data of **5** was collected on Gemini R-Ultra single crystal diffractometer CCD from Oxford Diffraction equipped with Ruby detector using Mo$K\alpha$ radiation with graphite monochromatization (λ = 0.71073 Å). Determination of the unit cells and data collection was carried out at 150 K for **1** and at 121 K for **5.** The structures were solved by direct methods and refined against F^2 using the ShelXL program[104] run under WinGX[105].

Non-hydrogen atoms were refined with anisotropic displacement parameters; hydrogen atoms were usually refined using the isotropic model with U_{iso}(H) values fixed at 1.5 U_{eq} of the C atoms for $^-CH_3$ or 1.2 U_{eq} for ^-CH, $^-CH_2$ groups and aromatic H.

The voids in the crystal structure of **3** contain disordered $[Li(dme)_3]^+$ counterion and a half of free DME molecule (four $[Li(dme)_3]^+$ counterions and two DME molecules in the unit cell), in the crystal structure of **4** contain disordered pentane molecule (6 pentane molecules in the unit cell) and in the crystal structure of **5** contain disordered $[Li(dme)_3]^+$ counterion (four $[Li(dme)_3]^+$ counterions in the unit cell). A satisfactory model for the disordered molecules in **3**, **4**, and **5** was not found, and therefore the PLATON[106–109]/SQUEEZE[110] program was used to mask out the disordered density.

Crystallographic data for the structures of **1**-**5** reported in this paper have been deposited with the Cambridge Crystallographic Data Centre as supplementary publication No. CCDC 1911161-1911165. Copies of the data can be obtained free of charge on application to CCDC, 12 Union Road, Cambridge CB2 1EZ, UK (Fax: (+44) 1223-336-033; E-mail: deposit@ccdc.cam.ac.uk). For more crystallographic details see ESI.

The zero-field Mössbauer spectra recorded for **1**-**3** were obtained using a spectrometer equipped with a liquid-nitrogen cooled cryostat. The spectrometer was operated in a constant acceleration mode. The isomer shifts are reported against the centroid of a room-temperature spectrum recorded for a α-iron metal foil.

Elemental analyses were performed at the University of Gdańsk using a Vario El Cube CHNS apparatus. Li content in crystalline samples of complexes **1**-**3** was determined by microwave plasma - atomic emission spectrometry MP-AES (Table S4). The obtained crystals before Li determination had to be mineralized. The mineralization of crystal samples was carried out using 2M HNO_3 prepared by using 65% HNO_3 of pure grade (POCH) and distilled water. About 0.05 g of each crystal sample was weighted and 10 ml of 2M HNO_3 was added. Mineralization was carried out for 0.5 h at room temperature. Subsequently, the obtained sample solutions were filtered and diluted in volumetric flasks before the analysis. The total concentration of Li in analysed solutions of mineralized crystals was determined with the use of microwave plasma - atomic emission spectrometer, 4210 MP-AES supplied by Agilent. Calibration solution used was ICP grade. The measurements were performed in 4 repetitions and in 3 separate procedures with different wavelength. The wavelengths used for Li determination were as follows: 610.37 nm, 670.79 nm and 460.30 nm. Uncertainty is presented as standard uncertainty form all 12 measurements.

Synthetic procedures

$[FeBr_2(thf)_2]$: Anhydrous $FeBr_2$ (10 g, 0.046 mol) was placed in the Soxhlet extractor and extracted with 300 mL of THF over two days. The THF extract was then stored at RT yielding light orange crystals. Additional crops were obtained by cooling of the mother liquor to +4°C and then to -20°C. Yield: 13.5 g (0.037 mol, 81%).

General procedures for the syntheses of homoleptic phosphido complexes of iron

Method A: At -30°C, a DME solution of R_2PLi was added dropwise to a stirred suspension of $[(Dippnacnac)FeCl_2Li(dme)_2]$ in DME. The reaction mixture was allowed to warm up to room temperature and was stirred overnight. The almost black mixture was then concentrated to half of volume and filtered. Cooling the filtrate to -20°C gave colorless crystals of [(Dippnacnac)Li(dme)] (identified by ^{1}H NMR spectroscopy). Further crystallization of the mother liquor gave crystalline products suitable for X-ray crystallographic analysis. Crystals were isolated, washed with cold pentane at -50°C and dried *in vacuo.*

Method B: At -30°C, a DME solution of R_2PLi was added at once to a stirred suspension of $[FeBr_2(thf)_2]$ in DME. The reaction mixture was allowed to warm up to room temperature and stirred overnight. The mixture was then concentrated to half of volume and filtered. Cooling of the solution to -20°C gave colorless crystals, identified as LiBr by X-ray analysis. Further crystallization of the mother liquor gave crystalline products suitable for X-ray diffraction. Crystals were isolated, washed with cold pentane at -50°C and dried *in vacuo*.

$[Fe_2(\mu\text{-}PtBu_2)_2(PtBu_2)_2][Li(dme)_3]$ (1):

Method A: Reaction of 0.366 g (0.5 mmol) of $[(Dippnacnac)FeCl_2Li(dme)_2]$ in 2.5 mL of DME with 0.228 g (1.5 mmol) of tBu_2PLi in 4.5 mL of DME produced 0.047 g (yield 18%) of dark crystals (co-crystallized with LiCl in molar ratio 1:1). Single crystals were obtained by storing the DME filtrate (concentrated to the half of volume) at +4°C. Cooling of the mother liquor to -20°C gave an additional crop.

Method B: Reaction of 0.180 g (0.5 mmol) of $[FeBr_2(thf)_2]$ in 2.5 mL of DME with 0.304 g (2 mmol) of tBu_2PLi in 9 mL of DME produced 0.172 g (yield 65%) of dark red needle-shaped crystals (co-crystallization with LiBr in molar ratio 1:1). Single crystals were obtained from the DME filtrate concentrate to half of its volume, which was stored at +4°C. Cooling of the mother liquor to -20°C gave an additional crop.

^{1}H NMR (THF-d_8): δ 23.76 (bs, 36H); -22.48 (bs, 36H) ppm. Evans μ_{eff} (THF-d_8, 298 K): 5.66 μ_B. Elemental Analysis (Found: C, 49.63; H, 9.636. Calc. for $C_{44}H_{102}Fe_2LiO_6P_4$ + LiBr: C, 50.01; H, 9.730).

$[Fe_2(\mu\text{-}PtBuPh)_3(PtBuPh)_2][Li(dme)_3](dme)_{0.25}$ (2):

Method A: Reaction of 0.183 g (0.25 mmol) of $[(Dippnacnac)FeCl_2Li(dme)_2]$ in 1 mL of DME with 0.129 g (0.75 mmol) of tBuPhPLi in 3.5 mL of DME produced 0.061 g (yield 39%) of black crystals (co-crystallization with LiCl in molar ratio 1:0.5). Single crystals were obtained at room temperature by slow diffusion of pentane (6 mL) into the as-obtained DME solution of the complex. Drying of the isolated crystals under high vacuum resulted in the removal of the non-coordinated DME molecule.

Method B: Reaction of 0.180 g (0.5 mmol) of $[FeBr_2(thf)_2]$ in 2.5 mL of DME with 0.258 g (1.5 mmol) of tBuPhPLi in 4.5 mL of DME produced 0.200 g (yield 64%) of almost black crystals (co-crystallization with LiBr in ratio 1:0.5). Single crystals were obtained at room temperature by slow diffusion of pentane (6 mL) into the as-obtained DME solution of the complex. Drying of the isolated crystals under high vacuum resulted in the removal of the non-coordinated DME molecule.

^{1}H NMR (THF-d_8): 39.79 (bs, 27H); 23.71 (bs, 9H); 20.23 (bs, 6H); 6.83 (bs, 4H); 1.33 (bs, 18H); -9.80 (bs, 6H) ppm. Evans μ_{eff} (THF-d_8, 298 K): 6.96 μ_B. Elemental Analysis (Found: C, 59.59; H, 8.097. Calc. for $C_{62}H_{100}Fe_2Li_1O_6P_5$ + 0.5 LiBr: C, 59.18; H, 8.010).

$[Fe_2(\mu\text{-}PCy_2)_3(PCy_2)_2][Li(dme)_3]\cdot(dme)_{0.5}$ (3):

Method A: Reaction of 0.366 g (0.5 mmol) of $[(Dippnacnac)FeCl_2Li(dme)_2]$ in 2.5 mL of DME with 0.306 g (1.5 mmol) of Cy_2PLi in 4.5 mL of DME produced 0.305 g (yield 86%) of dark violet crystals (co-crystallization with LiCl in molar ratio 1:1). Crystals were obtained from the concentrated DME filtrate (reduced to half of its initial volume), which was stored at +4°C. Cooling of the mother liquor to -20°C gave an additional crop. Drying of the isolated crystals under high vacuum resulted in the removal of the non-coordinated DME molecule.

Method B: Reaction of 0.090 g (0.25 mmol) of $[FeBr_2(thf)_2]$ in 2 mL of DME with 0.306 g (1.5 mmol) of Cy_2PLi in 4.5 mL of DME produced 0.015 g (yield 8%) of almost black crystals (co-crystallization with LiBr in ratio 1:1). Single crystals suitable for X-ray crystallographic analysis were obtained from concentrated DME filtrate (volume reduced to half) which was stored at +4°C. Cooling of the mother liquor to -20°C gave an additional crop. Drying of the isolated crystals under high vacuum resulted in the removal of the non-coordinated DME molecule.

^{1}H NMR (THF-d_8): 22.67 (bs, 36H); 11.63 (bs, 24H); 0.43 (bs, 24H); -0.66 (bs, 16H) ppm. Evans μ_{eff} (THF-d_8, 299 K): 6.89 μ_B. Elemental Analysis (Found: C, 60.93; H, 9.925. Calc. for $C_{72}H_{140}Fe_2LiO_6P_5$ + LiCl: C, 61.00; H, 9.953).

$[Fe_4(\mu\text{-}PiPr_2)_6](C_5H_{12})$ (4):

Method A: Reaction of 0.366 g (0.5 mmol) of $[(Dippnacnac)FeCl_2Li(dme)_2]$ in 2.5 mL of DME with 0.186 g (1.5 mmol) of iPr$_2$PLi in 4.5 mL of DME produced 0.070 g (yield 58%) of black crystals. Afterwards, the solvent was evaporated under high vacuum and the residue was washed with pentane (10 mL). Crystals were obtained from the concentrated pentane solution (initial volume reduced to half), which was stored at -70°C for 3 months. Drying of the isolated crystals under high vacuum resulted in the removal of the non-coordinated pentane molecule.

Method B: Reaction of 0.180 g (0.5 mmol) of $[FeBr_2(thf)_2]$ in 2.5 mL of DME with 0.186 g (1.5 mmol) of iPr$_2$PLi in 4.5 mL of DME produced 0.005 g (yield 3%) of almost black crystals. Afterwards, the solvent was evaporated under high vacuum and the residue was washed with pentane (10 mL). Single crystals suitable for X-ray crystallographic analysis were obtained from the pentane solution (concentrated by reducing half of its volume), which was stored at +4°C. Drying of the isolated crystals under high vacuum resulted in the removal of the non-coordinated pentane molecule.

Elemental Analysis (Found: C, 46.78; H, 9.029. Calc. for $C_{36}H_{84}Fe_4P_6$: C, 46.68; H, 9.141).

$[Fe(\eta^1\text{-}Me_3SiP\text{-}PtBu_2)_3][Li(dme)_3]$ (5): A solution of 0.338 g (0.910 mmol) of tBu$_2$PP(SiMe$_3$)Li·1.6THF in 3 mL of DME was added dropwise to a stirred suspension of 0.274 g (0.375 mmol) of $[(Dippnacnac)FeCl_2Li(dme)_2]$ in 1.5 mL of DME at -30°C. After warming to room temperature the almost black mixture was concentrated to the half of volume and filtered. Cooling the filtrate to -20°C of the solution gave colorless crystals of [(Dippnacnac)Li(dme)] (identified by ^{1}H NMR spectroscopy). Further crystallization by slow diffusion of pentane (3 mL) into the obtained mother liquor at room temperature gave 0.140 g (yield 32%) of dark brown crystals (co-crystallization with LiCl in molar ratio 1:2).

Elemental Analysis (Found: C, 46.59; H, 9.168. Calc. for $C_{45}H_{111}FeLiO_6P_6Si_3$ + 2LiCl: C, 46.35; H, 9.595).

Conflicts of interest

There are no conflicts to declare.

Acknowledgements

K.K. obtained financial support from the National Science Centre NCN, Poland (ETIUDA 6, no. 2018/28/T/ST5/00120) as a part of the doctoral scholarship. K.K. thanks Prof. Hans-Jörg Krüger and Dr. Harald Kelm for an internship opportunity (Project 'Inter PhD' no. POKL.04.01.01-00-368/09) and for their guidance and supervision. Mössbauer spectra were recorded at NHMFL which is supported by the NSF award DMR-1644779 and the State of Florida. This work was also supported in part by start-up funds from the University of Idaho to S.A.S.

Notes and references

1 S. L. Brock, S. C. Perera and K. L. Stamm, *Chem. Eur. J.*, 2004, **10**, 3364–3371.
2 R. Prins and M. E. Brussell, *Catal. Lett.*, 2012, **142**, 1413–1436.
3 J. F. Callejas, C. G. Read, C. W. Roske, N. S. Lewis and R. E. Schaak, *Chem. Mater.*, 2016, **28**, 6017–6044.
4 E. Muthuswamy, P. R. Kharel, G. Lawes and S. L. Brock, *ACS Nano*, 2009, **3**, 2383–2393.
5 C. T. Lo and P. Y. Kuo, *J. Phys. Chem. C*, 2010, **114**, 4808–4815.
6 N. Singh, P. K. Khanna and P. A. Joy, *J. Nanopart. Res.*, 2009, **11**, 491–497.
7 S. E. Habas, F. G. Baddour, D. A. Ruddy, C. P. Nash, J. Wang, M. Pan, J. E. Hensley and J. A. Schaidle, *Chem. Mater.*, 2015, **27**, 7580–7592.
8 L. Liu, Q. Li, Z. Wang, J. Yan and Y. Chen, *Funct. Mater. Lett.*
9 R. Kikuchi, T. Ataku, A. Takagaki and S. T. Oyama, *ECS Trans.*, 2016, **75**, 931–937.
10 Y.-M. Chun and H.-C. Shin, *Electrochim. Acta*, 2016, **209**, 369–378.
11 W. Zhang, M. Dahbi, S. Amagasa, Y. Yamada and S. Komaba, *Electrochem. commun.*, 2016, **69**, 11–14.
12 W.-J. Li, S.-L. Chou, J.-Z. Wang, H.-K. Liu and S.-X. Dou, *Chem. Commun.*, 2015, **51**, 3682–3685.
13 B. J. H. Stadler, K. Vaccaro, G. O. Ramseyer, E. A. Martin, H. M. Dauplaise, L. M. Theodore and J. P. Lorenzo, *J. Electron. Mater.*, 1996, **25**, 709–713.
14 P. W. Menezes, A. Indra, C. Das, C. Walter, C. Göbel, V. Gutkin, D. Schmeißer and M. Driess, *ACS Catal.*, 2017, **7**, 103–109.
15 J. F. Callejas, J. M. Mcenaney, C. G. Read, J. C. Crompton, A. J. Biacchi, E. J. Popczun, T. R. Gordon, N. S. Lewis and R. E. Schaak, *ACS Nano*, 2014, **8**, 11101–11107.
16 T. Zhang, J. Du, P. Xi and C. Xu, *ACS Appl. Mater. Interfaces*, 2017, **9**, 362–370.
17 S. Yao, V. Forstner, P. W. Menezes, C. Panda, S. Mebs, E. M. Zalnhofer, M. E. Miehlich, T. Szilvási, N. A. Kumar, M. Humann, K. Meyer, H. Grützmacher and M. Driess, *Chem. Sci.*, 2018, **9**, 8590–8597.
18 L. Rosenberg, *Coord. Chem. Rev.*, 2012, **256**, 606–626.
19 A. J. Carty, S. A. MacLaughlin and D. Nucciarone, *Methods Stereochem. Anal.*, 1987, **8**, 559–619.
20 H. Werner, *Comments Inorg. Chem.*, 1990, **10**, 267–295.
21 W. Wang, P. J. Low, A. J. Carty, E. Sappa, G. Gervasio, C. Mealli, A. Ienco and E. Perez-Carreño, *Inorg. Chem.*, 2000, **39**, 998–1005.
22 S. C. Goel, M. A. Matchett, D. Cha, M. Y. Chiang and W. E. Buhro, *Phosphorus. Sulfur. Silicon Relat. Elem.*, 1993, **76**, 289–292.
23 G. W. Rabe, G. P. A. Yap and A. L. Rheingold, *Inorg. Chem.*, 1997, **36**, 3212–3215.
24 W. Clegg, K. Izod and S. T. Liddle, *J. Organomet. Chem.*, 2000, **613**, 128–131.
25 A. Schisler, P. Lönnecke, U. Huniar, R. Ahlrichs and E. Hey-Hawkins, *Angew. Chem. Int. Ed.*, 2001, **40**, 4217–4219.
26 A. Schisler, P. Lönnecke and E. Hey-Hawkins, *Inorg. Chem.*, 2005, **44**, 461–464.
27 S. Gómez-Ruiz, A. Schisler, P. Lönnecke and E. Hey-Hawkins, *Chem. Eur. J.*, 2007, **13**, 7974–7982.
28 S. Gomez-Ruiz and E. Hey-Hawkins, *New J. Chem.*, 2010, **34**, 1525–1532.
29 A. Kırcalı Akdag, P. Lönnecke and E. Hey-Hawkins, *Z. Anorg. Allg. Chem.*, 2014, **640**, 271–274.
30 P. Coburger, S. Demeshko, C. Rödl, E. Hey-Hawkins and R. Wolf, *Angew. Chemie Int. Ed.*, 2017, **56**, 15871–15875.
31 J. Sugiura, T. Kakizawa, H. Hashimoto, H. Tobita and H. Ogino, *Organometallics*, 2005, **24**, 1099–1104.
32 A. M. Geer, Á. L. Serrano, B. De Bruin, M. A. Ciriano and C. Tejel, *Angew. Chemie Int. Ed.*, 2015, **54**, 472–475.
33 Á. L. Serrano, M. A. Casado, M. A. Ciriano, B. De Bruin, J. A. López and C. Tejel, *Inorg. Chem.*, 2016, **55**, 828–839.
34 M. Itazaki, S. Katsube, M. Kamitani and H. Nakazawa, *Chem. Commun.*, 2016, **52**, 3163–3166.
35 V. Koshti, S. Gaikwad and S. H. Chikkali, *Coord. Chem. Rev.*, 2014, **265**, 52–73.
36 L. Rosenberg, *ACS Catal.*, 2013, **3**, 2845–2855.
37 D. S. Glueck, *Top. Organomet. Chem.*, 2010, **31**, 65–100.
38 R. Waterman, *Dalton Trans.*, 2009, 18–26.
39 D. S. Glueck, *Chem. Eur. J.*, 2008, **14**, 7108–7117.
40 D. S. Glueck, *Dalton Trans.*, 2008, 5276–5286.
41 M. Kamitani, M. Itazaki, C. Tamiya and H. Nakazawa, *J. Am. Chem. Soc.*, 2012, **134**, 11932–11935.
42 C. A. Bange and R. Waterman, *Chem. Eur. J.*, 2016, **22**, 12598–12605.
43 Y. S. Ganushevich, V. A. Miluykov, F. M. Polyancev, S. K. Latypov, P. Lönnecke, E. Hey-Hawkins, D. G. Yakhvarov and O. G. Sinyashin, *Organometallics*, 2013, **32**, 3914–3919.
44 C. A. Jaska, A. Bartole-Scott and I. Manners, *Dalton Trans.*, 2003, 4015–4021.
45 E. M. Leitao, T. Jurca and I. Manners, *Nat. Chem.*, 2013, **5**, 817–829.
46 R. Waterman, *Chem. Soc. Rev.*, 2013, **42**, 5629–5641.
47 P. Mastrorilli, *Eur. J. Inorg. Chem.*, 2008, 4835–4850.
48 X. Y. Yang, J. H. Gan, Y. Li, S. A. Pullarkat and P. H. Leung, *Dalt. Trans.*, 2014, **44**, 1258–1263.
49 I. Kovacik, C. Scriban and D. S. Glueck, *Organometallics*, 2006, **25**, 536–539.
50 R. L. Webster, *Dalton Trans.*, 2017, **46**, 4483–4498.
51 M. Espinal-Viguri, A. K. King, J. P. Lowe, M. F. Mahon and R. L. Webster, *ACS Catal.*, 2016, **6**, 7892–7897.

52 N. T. Coles, M. F. Mahon and R. L. Webster, *Organometallics*, 2017, **36**, 2262–2268.
53 A. K. King, A. Buchard, M. F. Mahon and R. L. Webster, *Chem. Eur. J.*, 2015, **21**, 15960–15963.
54 A. K. King, K. J. Gallagher, M. F. Mahon and R. L. Webster, *Chem. Eur. J.*, 2017, **23**, 9039–9043.
55 M. Espinal-Viguri, M. F. Mahon, S. N. G. Tyler and R. L. Webster, *Tetrahedron*, 2017, **73**, 64–69.
56 K. J. Gallagher, M. Espinal-Viguri, M. F. Mahon and R. L. Webster, *Adv. Synth. Catal.*, 2016, **358**, 2460–2468.
57 M. Espinal-Viguri, C. R. Woof and R. L. Webster, *Chem. Eur. J.*, 2016, **22**, 11605–11608.
58 K. Kaniewska, A. Dragulescu-Andrasi, Ł. Ponikiewski, J. Pikies, S. A. Stoian and R. Grubba, *Eur. J. Inorg. Chem.*, 2018, 4298–4308.
59 J. K. Pagano, C. A. Bange, S. E. Farmiloe and R. Waterman, *Organometallics*, 2017, **36**, 3891–3895.
60 A. M. Lunsford, J. H. Blank, S. Moncho, S. C. Haas, S. Muhammad, E. N. Brothers, M. Y. Darensbourg and A. A. Bengali, *Inorg. Chem.*, 2016, **55**, 964–973.
61 M. H. Cheah, S. J. Borg, M. I. Bondin and S. P. Best, *Inorg. Chem.*, 2004, **43**, 5635–5644.
62 H. C. Mun, S. J. Borg and S. P. Best, *Inorg. Chem.*, 2007, **46**, 1741–1750.
63 A. Rahaman, C. Gimbert-Suriñach, A. Ficks, G. E. Ball, M. Bhadbhade, M. Haukka, L. Higham, E. Nordlander and S. B. Colbran, *Dalt. Trans.*, 2017, **46**, 3207–3222.
64 R. Grubba, Ł. Ponikiewski, Ł. Tomorowicz and J. Pikies, *Acta Crystallogr. Sect. E Struct. Reports Online*, 2010, **E66**, m707.
65 R. Grubba, A. Wiśniewska, K. Baranowska, E. Matern and J. Pikies, *Dalton Trans.*, 2011, **40**, 2017–24.
66 R. Grubba, A. Wiśniewska, K. Baranowska, E. Matern and J. Pikies, *Polyhedron*, 2011, **30**, 1238–1243.
67 R. Grubba, K. Baranowska, D. Gudat and J. Pikies, *Organometallics*, 2011, **30**, 6655–6660.
68 A. Łapczuk-Krygier, K. Baranowska, Ł. Ponikiewski, E. Matern and J. Pikies, *Inorganica Chim. Acta*, 2012, **387**, 361–365.
69 T. Kruczyński, R. Grubba, K. Baranowska and J. Pikies, *Polyhedron*, 2012, **39**, 25–30.
70 M. Zauliczny, R. Grubba, Ł. Ponikiewski and J. Pikies, *Polyhedron*, 2017, **123**, 353–360.
71 Ł. Ponikiewski, A. Ziółkowska and J. Pikies, *Inorg. Chem.*, 2017, **56**, 1094–1103.
72 Ponikiewski, A. Ziółkowska, M. Zauliczny and J. Pikies, *Polyhedron*, 2017, **137**, 182–187.
73 R. Grubba, K. Kaniewska, Ł. Ponikiewski, B. Cristóvão, W. Ferenc, A. Dragulescu-Andrasi, J. Krzystek, S. A. Stoian and J. Pikies, *Inorg. Chem.*
74 A. M. Arif, A. H. Cowley, M. Pakulski, M.-A. Pearsall, W. Clegg, N. C. Norman and A. G. Orpen, *J. Chem. Soc., Dalt. Trans.*, 1988, 2713–2721.
75 R. A. Jones, A. L. Stuart, J. L. Atwood, W. E. Hunter and R. D. Rogers, *Organometallics*, 1982, **1**, 1721–1723.
76 H. Hashimoto, K. Kurashima, H. Tobita and H. Ogino, *J. Organomet. Chem.*, 2004, **689**, 1481–1495.
77 H.-C. Böttcher, A. Krug and H. Hartung, *Polyhedron*, 1995, **14**, 901–905.
78 W. F. Smith, J. Yule, N. J. Taylor, H. N. Paik and A. J. Carty, *Inorg. Chem.*, 1977, **16**, 1593–1600.
79 B. Walther, H. Hartung, J. Reinhold, P. G. Jones, C. Mealli, H. Bottcher, U. Baumeister, A. Krug and A. Moeckel, *Organometallics*, 1992, **11**, 1542–1549.
80 R. E. Ginsburg, J. M. Berg, R. K. Rothrock, J. P. Collman, K. O. Hodgson and L. F. Dahl, *J. Am. Chem. Soc.*, 1979, **101**, 7218–7231.
81 Y.-C. Shi and D.-C. Yang, Wei, Shi, Ying, Cheng, *J. Coord. Chem.*, 2014, **67**, 2330–2343.
82 M. R. Adams, G. Judith, W. Andrew and G. J. Long, *Inorg. Chem.*, 1992, **31**, 2–4.
83 W. Clegg, *Inorg. Chem*, 1976, **15**, 2928–2931.
84 D. Seyferth, T. G. Wood and R. S. Henderson, *J. Organomet. Chem.*, 1987, **336**, 163–182.
85 B. Walther, H. Hartung, J. Reinhold, P. G. Jones, H.-C. Böttcher, U. Baumeister and A. Krug, *Chem. Ber.*, 1992, **125**, 1379–1382.
86 H.-C. Böttcher, P. Mayer and T. Mayer, *Zeitschrift für Anorg. und Allg. Chemie*, 2013, **639**, 2609–2611.
87 *CSD v. 5.39*, update September 2018.
88 F. A. Cotton, L. M. Daniels, L. R. Falvello, J. H. Matonic and C. A. Murillo, *Inorganica Chim. Acta*, 1997, **256**, 269–275.
89 A. Klose, E. Solari, C. Floriani, A. Chiesi-Villa, C. Rizzoli and N. Re, *J. Am. Chem. Soc.*, 1994, **116**, 9123–9135.
90 F. A. Cotton, L. M. Daniels, J. H. Matonic and C. A. Murillo, *Inorganica Chim. Acta*, 1997, **256**, 277–282.
91 T. Nguyen, W. A. Merrill, C. Ni, H. Lei, J. C. Fettinger, B. D. Ellis, G. J. Long, M. Brynda and P. P. Power, *Angew. Chemie - Int. Ed.*, 2008, **47**, 9115–9117.
92 C. R. Hess, T. Weyhermüller, E. Bill and K. Wieghardt, *Angew. Chemie Int. Ed.*, 2009, **48**, 3703–3706.
93 C. M. Zall, D. Zherebetskyy, A. L. Dzubak, E. Bill, L. Gagliardi and C. C. Lu, *Inorg. Chem.*, 2012, **51**, 728–736.
94 S. Kuppuswamy, T. M. Powers, B. M. Johnson, M. W. Bezpalko, C. K. Brozek, B. M. Foxman, L. A. Berben and C. M. Thomas, *Inorg. Chem.*, 2013, **52**, 4802–4811.
95 S. J. Tereniak, R. K. Carlson, L. J. Clouston, V. G. Young, E. Bill, R. Maurice, Y. S. Chen, H. J. Kim, L. Gagliardi and C. C. Lu, *J. Am. Chem. Soc.*, 2014, **136**, 1842–1855.
96 P. Pyykkö and M. Atsumi, *Chem. Eur. J.*, 2009, **15**, 186–197.
97 L. Weber, S. Buchwald, D. Lentz, O. Stamm, D. Preugschat and R. Marschall, *Organometallics*, 1994, **13**, 4406–4412.
98 P. L. Holland, *Acc. Chem. Res.*, 2008, **41**, 905–914.
99 D. F. Evans, *J. Chem. Soc.*, 1959, 2003–2005.
100 G. A. Bain and J. F. Berry, *J. Chem. Educ.*, 2008, **85**, 532–536.
101 C. M. Zall, D. Zherebetskyy, A. L. Dzubak, E. Bill, L. Gagliardi and C. C. Lu, *Inorg. Chem.*, 2012, **51**, 728–736.
102 P. Gütlich, E. Bill and A. Trautwein, *Mössbauer spectroscopy and transition metal chemistry: fundamentals and application*, Springer, Berlin ; Heidelberg, 2011.
103 S. J. Yoo, H. C. Angove, B. K. Burgess, M. P. Hendrich and E. Münck, *J. Am. Chem. Soc.*, 1999, **121**, 2534–2545.
104 G. M. Sheldrick, *Acta Crystallogr. Sect. C Struct. Chem.*, 2015, **C71**, 3–8.

105 L. J. Farrugia, *J. Appl. Crystallogr.*, 2012, **45**, 849–854.
106 A. L. Spek, *J. Appl. Crystallogr.*, 2003, **36**, 7–13.
107 A. L. Spek, *Acta Crystallogr. Sect. D Biol. Crystallogr.*, 2009, **D65**, 148–155.
108 A. L. Spek, *Inorganica Chim. Acta*, 2018, **470**, 232–237.
109 A. L. Spek, *Acta Crystallogr. Sect. E Crystallogr. Commun.*, 2020, **E76**, 1–11.
110 A. L. Spek, *Acta Crystallogr. Sect. C Struct. Chem.*, 2015, **C71**, 9–18.